https://doi.org/10.5194/egusphere-2026-2712
Preprint. Discussion started: 11 June 2026

Bedrock water storage regulates seasonal forest sensitivity to climatic water deficit

Tianqi Song [1, 2, 3], Qingyi Mu [1, 2, 3*], Jinlong Li [1, 2, 4], Yao Zhang [5], Xiangyang Sun [6], Hui Qian [4, 7], Da Huang [1, 2, 3], Jianbing Peng [1, 2, 3*]

[1] State Key Laboratory of Loess Science, Chang'an University, Xi'an, 710054, China

[2] Shaanxi Yellow River Scientific Research Institute, Chang'an University, Xi'an, 710054, China

[3] School of Geological Engineering and Geomatics, Chang'an University, Xi'an, 710054, China

[4] School of Water and Environment, Chang'an University, Xi'an 710054, Shaanxi, China

[5] College of Urban and Environmental Sciences Sci, Peking University, Beijing, 100871, China

[6] State Key Laboratory of Hydraulics and Mountain River Engineering, Sichuan University, Chengdu, 610065, China

[7] Key Laboratory of Subsurface Hydrology and Ecological Effects in Arid Region of the Ministry of Education, Chang'an University, Xi'an 710054, Shaanxi, China

*Corresponding authors (qingyimu@chd.edu.cn; dicexy_1@126.com)

https://doi.org/10.5194/egusphere-2026-2712
Preprint. Discussion started: 11 June 2026

Abstract

Understanding how subsurface water storage regulates ecosystem responses to hydroclimatic variability is central to ecohydrology, but the extent to which lithology mediates seasonal sensitivity of forests to climatic water deficit (CWD) through soil–regolith water storage remains poorly understood. Using four satellite vegetation metrics and meteorological reanalysis (2000–2023), we quantify seasonal sensitivity to CWD across the hydro-lithological regions of the Qinling Mountains. Results show that forest functional responses to CWD were more pronounced than structural greenness, implying that greenness-based metrics may overlook substantial drought impacts on forest ecosystems. Temperature and precipitation affected drought sensitivity in different ways across seasons and regions. Higher temperatures generally reduced drought sensitivity in spring and summer, especially where soils and bedrock can store more water, but increased sensitivity in autumn. More precipitation increased sensitivity to CWD in summer and autumn, although this effect differed across regions. Bedrock-stored water exerts a dual effect. In summer, it helped reduce drought stress by providing extra water during the growing season. In spring, however, it could increase vegetation sensitivity because it encouraged canopy development, which raised water demand. In regions where access to bedrock water was limited, even a small amount of bedrock-water access was associated with higher sensitivity to CWD. Our findings demonstrate that drought assessment and forest management should account for hydro-lithological properties and bedrock water dynamics.

Keywords: Bedrock water storage; Climatic water deficit; Hydro-lithological properties; Forest drought sensitivity; Qinling Mountains

https://doi.org/10.5194/egusphere-2026-2712
Preprint. Discussion started: 11 June 2026

1. Introduction

Hydroclimatic extremes driven by climate change increasingly challenge terrestrial ecosystems (Piao et al., 2019), but observed global greening does not necessarily translate resilience (Wu et al., 2025). Crucially, increasing water stress is decoupling ecosystem function from canopy greenness (Jiao et al., 2021), with evidence showing widespread losses of resilience to climatic water deficit (CWD) even amid biomass gains (Wang et al., 2023; Wu et al., 2025). Therefore, identifying the properties that influence vegetation sensitivity to water deficits is critical for predicting future carbon–water feedback (Dong et al., 2023; McDowell et al., 2020).

Conventionally, soil moisture has been evaluated as the primary water source for vegetation responses to climate variability because it supplies water for transpiration and buffers atmospheric evaporative demand (Miguez-Macho & Fan, 2021; Sun et al., 2025). However, emerging evidence shows that plants routinely retrieve water from weathered bedrock underlying the soil layer (McCormick et al., 2021). These deep reservoirs effectively buffer vegetation against short-term water deficits (Fan et al., 2017; Hahm et al., 2020; Y. Liu et al., 2025; Luo et al., 2024; Rempe & Dietrich, 2018; Schmidt & Rempe, 2020). However, bedrock-water access does not fundamentally enhance ecosystem resilience. In some landscapes, favourable subsurface moisture can promote vegetation expansion beyond a sustainable water supply, which increases transpiration demand and accelerates depletion of accessible storage; ultimately, sensitivity to subsequent deficits is amplified (Callahan et al., 2022; Hahm et al., 2019; Hahm et al., 2014; Zhang et al., 2024). This dual effect reflects lithology-driven contrasts in subsurface storage, recharge and hydraulic connectivity, which

https://doi.org/10.5194/egusphere-2026-2712
Preprint. Discussion started: 11 June 2026

regulate the trade-off between buffering and vulnerability.

Despite growing recognition that subsurface hydrology exerts bottom-up control on drought responses, two gaps persist. Firstly, vegetation sensitivity to water deficit is inherently phenology dependent because water demand and physiological regulation shift across the growing season (Wu et al., 2022). As a result, the same subsurface properties may buffer stress in one period but intensify vulnerability in another. However, many studies aggregate responses across the growing season, which potentially obscures intra-seasonal shifts driven by phenology–lithology interactions. Secondly, much of the evidence for bedrock-water dependence comes from Mediterranean-type climates, where precipitation and peak temperature are asynchronous, which makes reliance on deep reservoirs more apparent (Hahm et al., 2020; Leite et al., 2025). In monsoon-dominated montane regions, hydrothermal synchrony can support dense canopies and high transpiration demand, but intermittent rainfall and subsurface hydraulic constraints may lead to the demand–supply mismatch (Lian et al., 2024). Moreover, drought impacts are often inferred from canopy greenness, even though canopy-scale functioning varies substantially while structural greenness changes slightly. This misalignment motivates an explicit comparison of structural and functional responses under the same hydroclimatic forcing.

Here, we combine an ensemble of remotely sensed vegetation indicators with meteorological reanalysis (2000–2023) to examine the regulating effect of lithology–climate interactions on seasonal sensitivity to CWD in the Qinling Mountains, China's 'Central Water Tower'. We classify the region into three hydro-lithological domains (HS-HR, LS-HR and LS-LR) based on plant-available water capacity in soil and regolith (see in Method; H/L denotes

https://doi.org/10.5194/egusphere-2026-2712
Preprint. Discussion started: 11 June 2026

high/low, S/R denotes soil/regolith). We also quantify the variation in seasonal vegetation sensitivity to CWD across these regions. Using statistical analyses and scenario-based modelling, we further disentangle the interaction mechanism between bedrock-water access and seasonal climate variability to shape vegetation sensitivity to CWD across the growing season. The assessment uses structural greenness (NDVI and EVI) and functional activity (GPP and SIF). We demonstrate that the effect of bedrock water depends jointly on seasonal hydroclimate and lithology-driven hydraulic properties. This insight provides a mechanistic basis for assessing ecosystem stability under increasingly variable monsoon hydroclimate.

https://doi.org/10.5194/egusphere-2026-2712
Preprint. Discussion started: 11 June 2026

2. Methods

2.1 Study area

This study focuses on the Qinling Mountains in central China (30–36°N, 102–115°E; Figure 1a). The Qinling Mountains lie along China's north–south climate transition, which broadly separates humid from semi-humid climates. Moreover, the Qinling Mountains function as the China's central water tower, which supplies runoff that supports major inter-basin water transfers, including the Middle Route of the South-to-North Water Diversion Project.

Land cover includes forests (needleleaf and broadleaf) and non-forest types (e.g. grassland and shrubland; Figure 5a). Within the study area, needleleaf and broadleaf forests cover 12.3% and 23.7% of the land area, respectively. Climate is dominated by the monsoon system, in which summer moisture is delivered mainly by the South Asian and East Asian monsoons, and winter is influenced by the mid-latitude westerlies (Figure 1a). Annual precipitation ranges from 600 to 1000 mm (Figure 1d), with the majority occurring between June and September (Figure 1c), thereby creating a strong seasonal coupling between water supply and energy availability.

The geological context of Qinling Mountains is highly heterogeneous, with elevations ranging from low foothills below 46 m to high mountain ridges exceeding 5,202m (Figure 1b). Geologically, the Qinling Mountains originated from the prolonged collision and amalgamation of the North China Craton and the Yangtze Craton (Chen et al., 2025; Liu et al., 2023), and subsequent tectonic activity further enhanced spatial variability in altitude and bedrock composition (Figure 1e). This complex geology determines the hydraulic properties of soil and regolith layers, which influence vegetation root distribution, water uptake strategies and drought responses (Fan et al., 2017; Miguez-Macho & Fan, 2021; Ott, 2020; Stocker et al.,

https://doi.org/10.5194/egusphere-2026-2712
Preprint. Discussion started: 11 June 2026

2023).

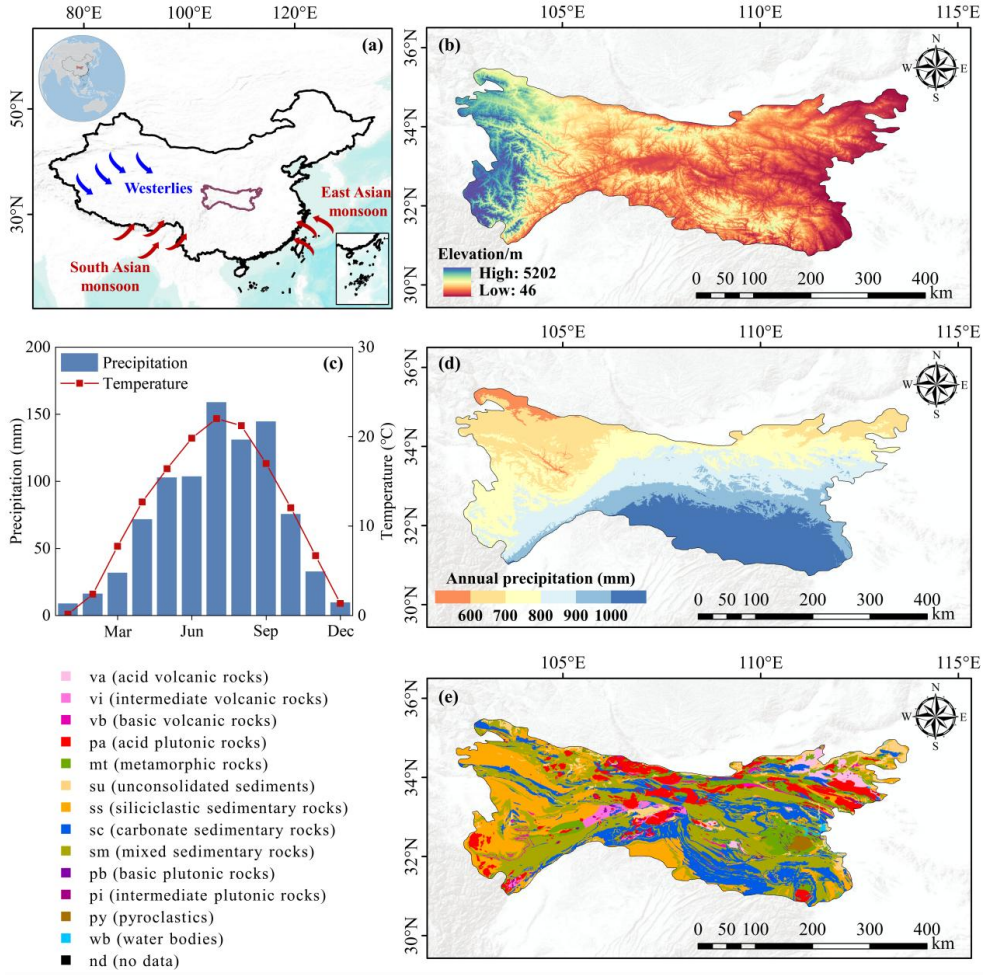

Figure 1 Distribution map of study units. (a) Location of the Qinling Mountains in China and the dominant circulation systems influencing the region; (b) Elevation of the Qinling Mountains; (c) Monthly mean precipitation (bars; mm) and temperature (line; °C) averaged over the period of 2000–2023; (d) Spatial distribution of annual precipitation; (e) Spatial distribution of lithologic units in the Qinling Mountains based on the Global Lithological Map database (GLiM) (Hartmann & Moosdorf, 2012)

https://doi.org/10.5194/egusphere-2026-2712
Preprint. Discussion started: 11 June 2026

2.2 Dataset

We obtained the Normalised Difference Vegetation Index (NDVI; 250 m resolution) dataset (Gao et al., 2023) in the period of 2000–2023 from the National Tibetan Plateau Data Centre. Solar-induced chlorophyll fluorescence (SIF; 0.05° resolution) data were derived from the LHSIF dataset (Zou et al., 2025). Moderate Resolution Imaging Spectroradiometer (MODIS) products (Running et al., 2021), including the Enhanced Vegetation Index (EVI; 500 m) and Gross Primary Productivity (GPP; 500 m), were sourced from the National Aeronautics and Space Administration. To systematically contrast canopy structural and functional responses to CWD, we categorised NDVI and EVI as structural indicators, while GPP and SIF were classified as functional indicators.

Monthly climatic variables for the period of 2000–2023, including precipitation (P), mean temperature (T) and potential evapotranspiration (PET) at 1 km resolution, alongside actual evapotranspiration (ET) at 500 m resolution, were obtained from established meteorological datasets (Ding & Peng, 2020, 2021; Peng et al., 2017, 2018, 2019). Monthly CWD was calculated as the difference between PET and ET (i.e., PET − ET).

Spatial distribution of vegetation types was extracted from the 1:1,000,000 scale Vegetation Map of China, which was provided by the Resources and Environmental Science Data Center. To estimate plant-available soil water storage, we utilised soil hydraulic properties and soil thickness data. Soil hydraulic properties were obtained from HiHydroSoil v2.0, a global gridded database of soil hydraulic properties at 250 m resolution (Simons et al., 2020). Soil thickness was obtained from the China High-resolution National Soil Information Grids, which provide high-resolution gridded soil property information for China, including soil thickness

https://doi.org/10.5194/egusphere-2026-2712
Preprint. Discussion started: 11 June 2026

and other basic soil attributes (Liu et al., 2022). Soil texture information was also based on the high-resolution three-dimensional soil texture mapping of China developed by Liu et al. (2020). Within the upper 2 m soil profile, available water content for each of the six standard depths (0–5, 5–15, 15–30, 30–60, 60–100, 100–200 cm) was determined by the difference between field capacity and the permanent wilting point. These interval values were weighted by layer thickness and integrated over the soil profile to compute the total plant-available water capacity (AWC) for each grid cell.

To ensure spatial alignment across all datasets, we resampled continuous variables (NDVI, EVI, GPP, SIF, AWC and climate fields) to a uniform 0.01° × 0.01° grid using bilinear interpolation. Categorical variables, including vegetation types and lithological units, were concurrently resampled to the identical resolution using a nearest-neighbour approach.

2.3 Masking procedures

To isolate forest ecosystems and ensure the fidelity of hydrological flux estimations, we implemented three successive masking criteria. Firstly, forest-dominated landscapes, comprising needleleaf and broadleaf taxa, were delineated based on resampled vegetation datasets (Figure 5a). Secondly, we narrowed the analysis to regions where cumulative evapotranspiration (ET) remained below cumulative precipitation (P) over the study period of 2000–2023. This criterion excludes areas exhibiting an unphysical long-term water deficit, which may stem from unquantified hydrological subsidies, such as occult precipitation (fog and dew), irrigation or lateral subsurface flow, that would otherwise confound the interpretation of the water balance. Furthermore, we excluded regions classified as unconsolidated sediments (su) and pyroclastic (py) to mitigate potential biases arising from extreme hydrological

https://doi.org/10.5194/egusphere-2026-2712
Preprint. Discussion started: 11 June 2026

heterogeneity and atypical subsurface storage dynamics.

2.4 Identification of the hydro-lithological regions

To assess the influence of the hydrologic properties of soil and regolith on vegetation sensitivity to climatic water deficit (CWD), we delineated the hydro-lithological regions across the study area. These regions represent (i) soil plant-available water capacity and (ii) regolith water storage and transmission potential. Following the main analysis, soil water availability was quantified as available water capacity (AWC). Regolith properties were represented by porosity (n) and permeability (K) from the Global Hydrogeology Maps (GLHYMPS) 2.0 dataset (Gleeson et al., 2014). All continuous layers (AWC, K and n) were resampled to a 0.01° grid prior to classification to ensure spatial consistency with the subsequent regression analyses.

Firstly, we classified each lithological unit as high (HS) or low (LS) soil water capacity using the domain-mean AWC as the threshold. Given that porosity and permeability vary strongly among lithological units, we constructed a rank-based composite index to represent regolith water storage and transmission potential (Figure 2). For each lithological unit, we calculated mean porosity (n) and permeability (K) across all grid cells within that unit. We converted n and K to ordinal scores by ranking the 12 lithological classes from highest to lowest for each property (scores 12–1). We then defined the regolith storage–transmission index (RSTI) as the sum of the porosity and permeability scores for each class. This unit-free index assumes that higher porosity (storage) and higher permeability (connectivity) jointly indicate a greater potential for plant-accessible water storage in the regolith. Lastly, we classified lithological units as high (HR) or low (LR) regolith storage–transmission potential using the mean RSTI as the threshold.

https://doi.org/10.5194/egusphere-2026-2712
Preprint. Discussion started: 11 June 2026

We combined soil (HS/LS) and regolith (HR/LR) classes to delineate three coupled hydro-lithological regions: HS–HR (mt, pi, va), LS–HR (vb, pb, sc) and LS–LR (vi, pa, ss, sm). After the masking procedure (Methods) was applied, no HS–LR combination occurred; therefore, the classification comprised three region types. This co-occurrence suggests that, in the Qinling Mountains, high soil AWC is often associated with regolith characterised by relatively high porosity and permeability.

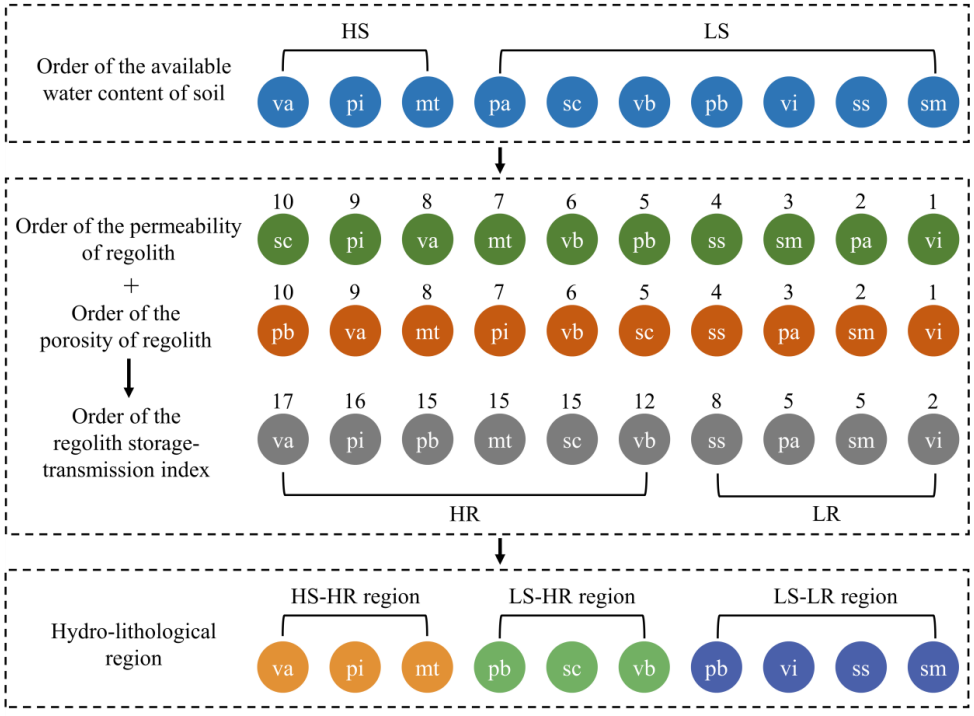

Figure 2 Schematic for identifying the hydro-lithological region.

2.5 Statistical analysis of vegetation sensitivity to CWD

To assess the impacts of CWD and hydroclimatic factors on vegetation structure, we employed a multiple linear regression model with interaction terms to disentangle the effects of precipitation (P) and temperature (T) on vegetation responses to water deficit. The model is

https://doi.org/10.5194/egusphere-2026-2712
Preprint. Discussion started: 11 June 2026

defined as follows:

$$y = \beta_0 + \beta_1 CWD + \beta_2 P + \beta_3 T + \gamma_1 (CWD \times P) + \gamma_2 (CWD \times T) + \alpha t + \epsilon \quad (1)$$

where y represents a vegetation indicator (NDVI, EVI, GPP, SIF, ensemble structural indicator or functional indicator).

To ensure comparability of regression coefficients across predictors and pixels, we first applied differencing, which removes the intercept term (β_0) from the model. After differencing, all variables (responses and predictors) were standardised to zero mean and unit variance after differencing. Thus, the coefficients represent changes in standard deviations of the vegetation indicator corresponding to a one-standard-deviation change in hydroclimatic drivers. Given the multicollinearity among CWD, climatic factors and their interaction terms, we employed ridge regression to estimate sensitivity parameters, as it constrains coefficient magnitudes to reduce variance and prevent overfitting. In the ridge regression, the coefficient β_1 reflects the ecosystem sensitivity at mean precipitation and temperature anomalies (P = 0, T = 0), which is defined as the change in a vegetation indicator per unit increases in CWD. Larger absolute values of sensitivity represent stronger vegetation response to water deficits. Notably, negative sensitivities indicate declines in vegetation activity under higher CWD, and positive sensitivities indicate increases. β_2, β_3, γ_1 and γ_2 denote the direct effects of precipitation and temperature on vegetation growth, and their marginal effects on vegetation sensitivity to CWD. The regressor t is an augment term to account for potential spurious regression due to trends in variables, which is preferred over explicit detrending methods for handling stochastic trends. We employed differencing to eliminate the constant β_0. Although monthly data were processed from 2000 to 2023, statistical analyses were limited to the growing season (March to

https://doi.org/10.5194/egusphere-2026-2712
Preprint. Discussion started: 11 June 2026

November).

2.6 Contributions of bedrock water storage to vegetation sensitivity

To estimate the contribution of bedrock-stored water to vegetation evapotranspiration, we applied a monthly storage-deficit water-balance framework for 2000–2023, following recent applications that infer below-soil water use from the mismatch between evapotranspiration demand and water supplied by precipitation and soil water storage (Ehlert et al., 2024; Qiu et al., 2026). This approach simulates plant-available soil water dynamics (S_{soil}), whereby any monthly ET demand exceeding precipitation and soil storage is attributed to bedrock water uptake ($S_{bedrock}$). We assumed preferential vegetation reliance on soil water and prioritised refilling of the soil reservoir by precipitation before any runoff or deep drainage occurs. The model operates continuously (non-resetting), which allows soil water deficits or surpluses to accumulate across monthly and inter-annual timescales. This continuous accounting captures the legacy effects of multi-year droughts and provides a conservative estimate of bedrock water use, as deeper sources are only accessed once soil water is exhausted.

For each grid cell, S_{soil} was initialised at AWC in January 2000. At each time step t, the model updated these stores as follows: precipitation (P_t) was added to the soil reservoir until AWC was reached, and water was removed from the soil to satisfy the monthly actual evapotranspiration (ET_t). If ET demand exceeded the sum of precipitation and the available soil water from the previous month, then the shortfall was met by bedrock water use ($S_{bedrock,t}$).

$$S_{bedrock,t} = max\left[0, ET_t - min\left(S_{soil}, S_{soil,t-1} + P_t\right)\right] \quad (2)$$

The soil water for the subsequent month (t+1) was then determined by the residual soil moisture following ET plus the surplus precipitation, with the total value bounded between zero

https://doi.org/10.5194/egusphere-2026-2712
Preprint. Discussion started: 11 June 2026

and the AWC:

$$S_{soil,t} = max\left[0, min\left(AWC, S_{soil,t-1} + P_t - ET_t\right)\right] \quad (3)$$

Lastly, we summed the monthly bedrock water ($S_{bedrock,t}$) over the period of 2000–2023 to obtain the cumulative plant available water capacity in bedrock for each grid cell ($S_{bedrock,cum}$). This iterative accounting captures the temporal propagation of moisture deficits during prolonged dry spells, which quantifies the magnitude of deep-seated water subsidies required to sustain transpirational demand when soil reserves are exhausted. This approach provides a conservative estimate of bedrock-water contribution because bedrock water is invoked only after shallow-soil water is depleted. In some ecosystems, however, plants can access bedrock water before shallow-soil water is exhausted (Qiu et al., 2026). Our estimates therefore probably represent a lower bound on the contribution of bedrock water to ET.

To evaluate the regulating effect of bedrock-water access on vegetation sensitivity to drought, we defined a counterfactual CWD without bedrock subsidy (CWD_e) as the atmospheric water demand that would remain unmet in the absence of inferred bedrock-stored water. In this framework, the conventional CWD underestimates potential ecological water stress when part of transpiration is sustained by bedrock water:

$$CWD_{e,y} = CWD_y + S_{bedrock,y} \quad (4)$$

We then re-estimated vegetation sensitivity by substituting CWD_e for CWD as the primary predictor in our regression framework. By comparing the sensitivity coefficient derived from CWD_e (β_{1e}) against the original CWD baseline (β_1), we quantified the extent to which bedrock water buffers ecosystem responses to moisture deficits.

https://doi.org/10.5194/egusphere-2026-2712
Preprint. Discussion started: 11 June 2026

3. Results and discussion

3.1 Seasonal decoupling between canopy structure and function

We partition the Qinling Mountains into three hydro-lithological regions based on plant-available water capacity in soil and regolith, and the data are inferred from available water content of soil and porosity/permeability of regolith (Gleeson et al., 2014). We define the HS-HR (high soil water availability, high regolith water availability), the LS-HR (low soil, high regolith) and the LS-LR (low soil, low regolith), which account for 13.6%, 18.8% and 67.6% of the study area, respectively (Figure 3a).

Across all hydro-lithological regions, functional activity showed generally stronger sensitivity to CWD than structural greenness, which reveals a pervasive functional–structural decoupling. During the growing season, functional indicator was positively sensitive to CWD in all regions and was highest in the LS-HR (0.11 to 0.14; Figure 3c), compared with the HS-HR region (0.04 to 0.10; Figure 3b) and the LS-LR region (0.00 to 0.09; Figure 3d). By contrast, structural sensitivity was weak (near zero) and generally negative across regions (−0.10 to 0.10). This difference likely arises because photosynthesis responds rapidly through stomatal and photochemical regulation, whereas canopy greenness exhibits slower processes such as carbon allocation and phenological development (Li et al., 2023; Nadal-Sala et al., 2021; Vicca et al., 2016; Xu et al., 2024). Consequently, changes in structural greenness under-represent concurrent shifts in canopy function under fluctuating water deficits. Furthermore, in these monsoon mountain ecosystems, the generally positive functional sensitivity suggests that moderate increases in CWD coincide with clearer skies and higher incoming radiation (Sreeparvathy et al., 2025; Yang et al., 2024). This radiative boost can transiently enhance

https://doi.org/10.5194/egusphere-2026-2712
Preprint. Discussion started: 11 June 2026

photosynthetic activity even when canopy greenness remains largely unchanged.

This functional–structural decoupling was strongly seasonal. Functional sensitivity to CWD decreases from 0.21 in spring to −0.03 in summer, before recovering to 0.06 in autumn (Figure 4). Among the functional indicators, the sign weakened in summer and autumn was driven mainly by GPP, which became negative in summer and persisted into autumn, whereas SIF maintained positive responses across seasons (Figure 4). By contrast, structural sensitivity remained feeble for most of the growing season, which shifted from 0.09 in spring to −0.09 in autumn. This observation is consistent with the view that structural greenness tracks slower phenological dynamics, whereas SIF- and GPP-based indicators capture faster physiological regulation (Zeng et al., 2023; Zhao et al., 2025). Structural sensitivity was positive in spring across all three regions. However, in LS-HR and LS-LR regions, where soil water availability is low, structural sensitivity became negative in summer, signalling a shift from energy limitation to water limitation during peak growth. This observation suggests that springtime greening can increase canopy evapotranspiration, which potentially makes vegetation in areas with low soil water availability more susceptible to water stress in summer (Lian et al., 2020; Zhang et al., 2025).

These divergent seasonal trajectories between structural greenness and functional activity are further supported by contrasting responses across forest types. Across all hydro-lithological regions, needleleaf and broadleaf forests show strong functional sensitivity to CWD, which peaks in the LS-HR region and declines as the season progresses (Figure 5). Compared with needleleaf forests, broadleaf forests show more negative structural sensitivity in summer and autumn, unveiling that greenness tracks water limitation more closely in broadleaf stands (Jin

https://doi.org/10.5194/egusphere-2026-2712
Preprint. Discussion started: 11 June 2026

et al., 2023; Liu et al., 2024). Overall, the strong functional sensitivity to CWD but weak (and often negative) structural sensitivity, especially in broadleaf stands in summer and autumn, reinforces that greenness alone is insufficient to diagnose functional responses to drought.

https://doi.org/10.5194/egusphere-2026-2712
Preprint. Discussion started: 11 June 2026

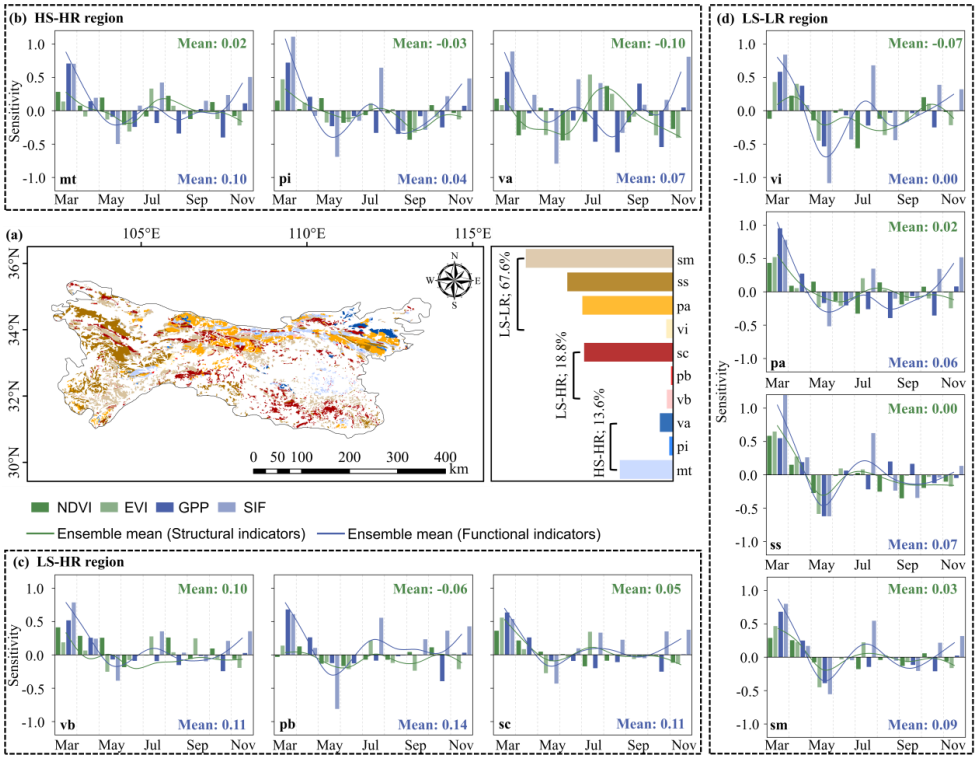

311

312 Figure 3 Hydro-lithological regions of the Qinling Mountains and monthly sensitivity of
313 vegetation indicators to CWD. (a) Map of hydro-lithological regions in the Qinling Mountains.
314 The bar chart shows the area fraction of each hydro-lithologic region. (b–d), Monthly sensitivity
315 of vegetation indicators to CWD in the HS-HR (b), LS-HR (c) and LS-LR (d) regions. Bars
316 show sensitivities of the four indicators (NDVI, EVI, GPP and SIF) to CWD for each lithologic
317 class. Solid lines show the ensemble-mean sensitivities of structural indicators (NDVI and EVI)
318 and functional indicators (GPP and SIF).

https://doi.org/10.5194/egusphere-2026-2712
Preprint. Discussion started: 11 June 2026

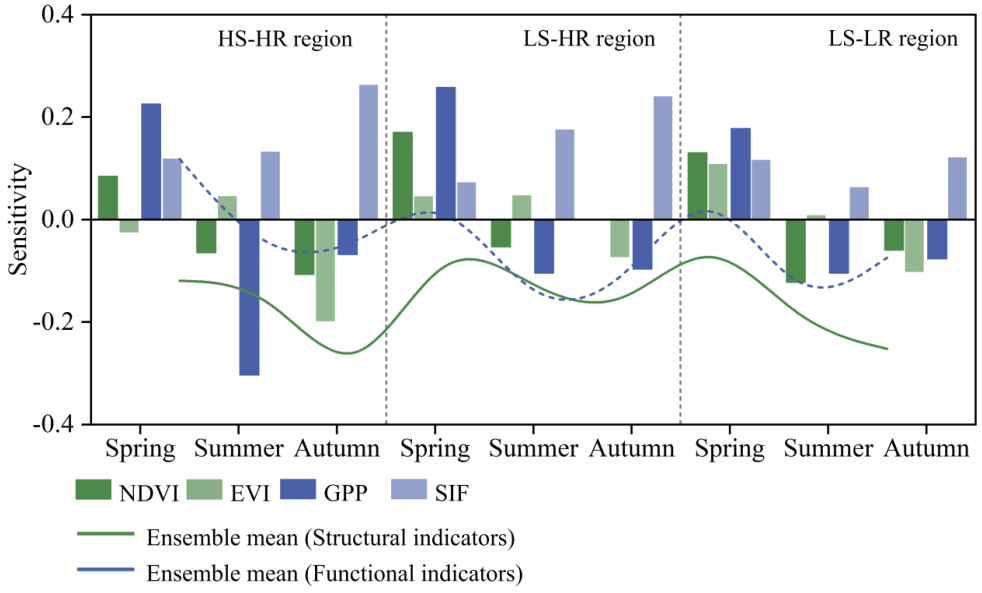

Figure 4 Seasonal sensitivity of vegetation indicators to CWD across three hydro-lithological regions

https://doi.org/10.5194/egusphere-2026-2712
Preprint. Discussion started: 11 June 2026

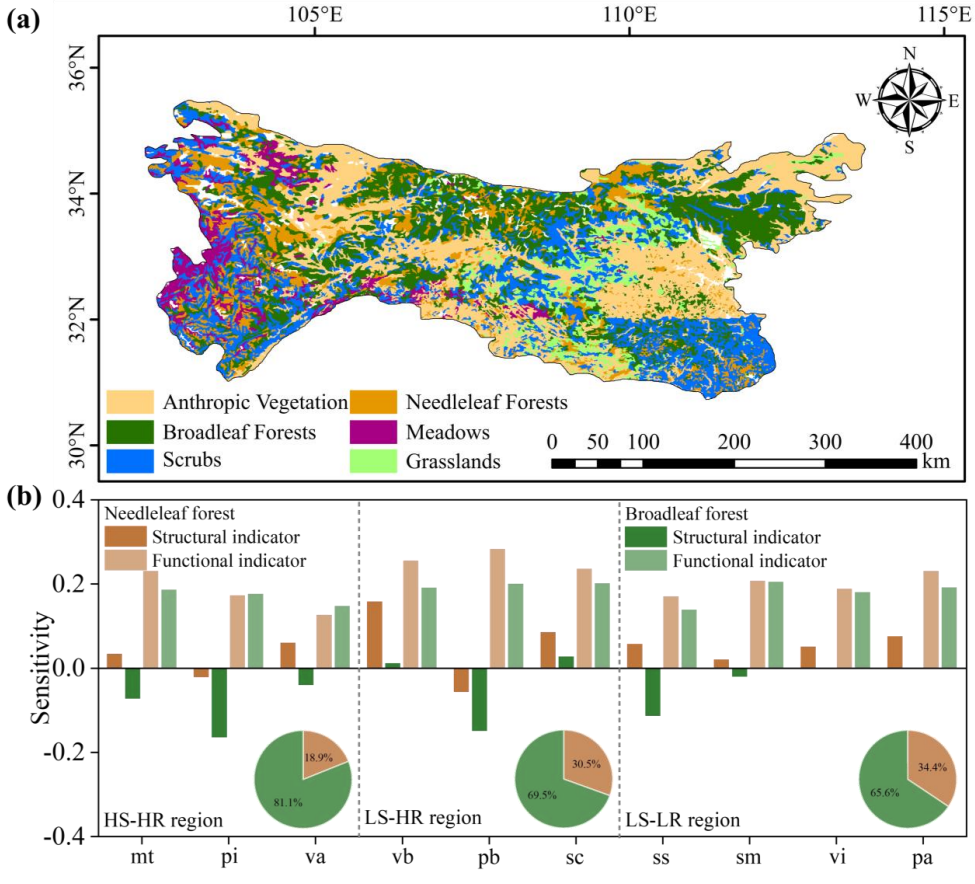

Figure 5 Vegetation patterns and forest sensitivity to climatic water deficit across hydro-lithological regions in the Qinling Mountains. (a) spatial distribution of vegetation types in the Qinling Mountains based on the 1:1,000,000 Vegetation Map of China from the National Cryosphere Desert Data Center; (b) mean sensitivity of needleleaf and broadleaf forests to climatic water deficit (CWD) across three hydro-lithological regions.

https://doi.org/10.5194/egusphere-2026-2712
Preprint. Discussion started: 11 June 2026

3.2 Seasonal climate regulation and marginal effects on CWD sensitivity

Temperature and precipitation influenced functional activity and structural greenness differently in magnitude and seasonality. In spring, structural greenness increased with temperature (mean effect = 0.31; Figure 6), which is consistent with earlier leaf-out and faster canopy development under warming (Jiang et al., 2024). This spring temperature signal was strongest in the HS-HR region, where higher soil and regolith water availability likely alleviate water limitation. By summer and autumn, this temperature effect on structural greenness waned. By contrast, temperature effects on functional indicators remained evident in all seasons and were strongest in autumn (mean effect = 0.46; Figure 6). In water-unlimited conditions, warming enhances photosynthetic rates; as a result, functional indicators show a clearer temperature response than structural greenness.

Precipitation exerted more complex control on vegetation growth than temperature (Figures 6 and 7). In spring, precipitation had a minuscule effect on canopy greenness (mean effect = 0.01–0.08). Nevertheless, precipitation can recharge shallow water stores during leaf-out, which eases plant water stress and supports turgor-driven growth (Tian et al., 2019; Zhang et al., 2025). Contrary to typical expectations, precipitation during the summer and autumn negatively correlates with vegetation greenness and functional activity, which suggests that excess precipitation fails to increase plant-available water. Prolonged wetness may induce transient anoxia, enhance nutrient leaching and reduce incoming radiation, which jointly constrain canopy greenness and functional activity (Dossa et al., 2019; Mokhtar et al., 2020). Consistent with this mechanism, precipitation suppressed summer functional activity in the water-rich HS-HR region, whereas its influence became weakly positive in the drier LS-HR

https://doi.org/10.5194/egusphere-2026-2712
Preprint. Discussion started: 11 June 2026

and LS-LR regions.

Precipitation and temperature not only affect vegetation growth directly but also regulate the structural and functional sensitivities to CWD. Across the growing season, functional and structural sensitivities increased with precipitation (marginal effects: 0.07–0.25 for functional indicator and 0.12–0.18 for structural indicator; Table 1). This finding suggests that additional precipitation further increased functional and structural sensitivity to CWD throughout the growing season. One explanation is that energy limitation in the Qinling Mountains (incoming radiation and temperature) constrains photosynthesis and evapotranspiration, such that additional water inputs do not fully translate into canopy growth (Condon et al., 2020; Fu et al., 2024). By contrast, temperature had generally negative marginal effects on functional and structural indicators during the early and peak growing-season periods, with the strongest effects in the water-sufficient HS–HR region (marginal effects: −0.09 to −0.03 for functional indicator and −0.32 to −0.07 for structural indicator; Table 1). Therefore, in areas with high water availability in regolith, the marginal effect of temperature on sensitivity to CWD diminished towards zero. However, the temperature marginal effect became positive in autumn, which implies that the availability of subsurface water allows higher temperatures to extend the window for photosynthesis (Keenan et al., 2014; Li et al., 2025). These marginal effect patterns are broadly consistent between individual indicators and ensemble indicators. On the contrary, the temperature marginal effect on SIF sensitivity remains positive in spring, summer and autumn (Table 1).

https://doi.org/10.5194/egusphere-2026-2712
Preprint. Discussion started: 11 June 2026

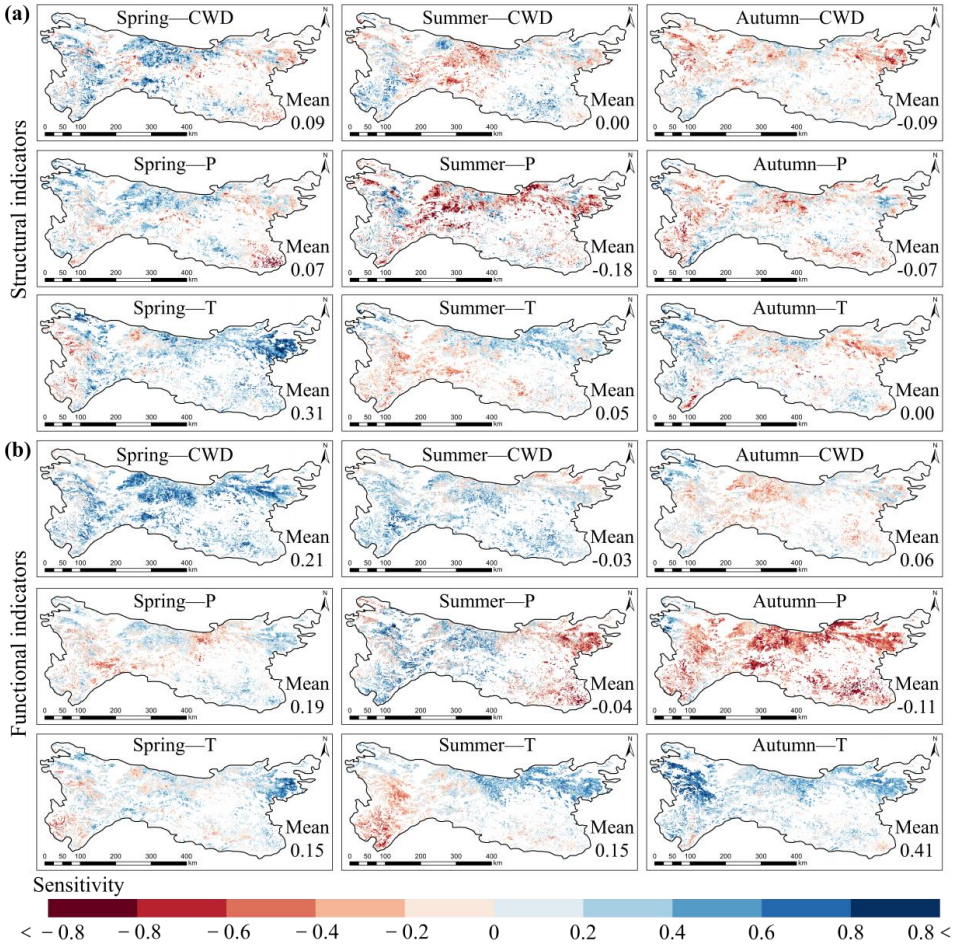

370

371 Figure 6 Spatial distribution and regional means of ridge-regression coefficients for climate
372 drivers. (a) Ridge-regression coefficients for structural indicators showing the sensitivities to
373 climatic water deficit (CWD; β_1), precipitation (P; β_2) and temperature (T; β_3) in spring, summer
374 and autumn; (b) Ridge-regression coefficients for functional vegetation indicators, as in (a)

https://doi.org/10.5194/egusphere-2026-2712
Preprint. Discussion started: 11 June 2026

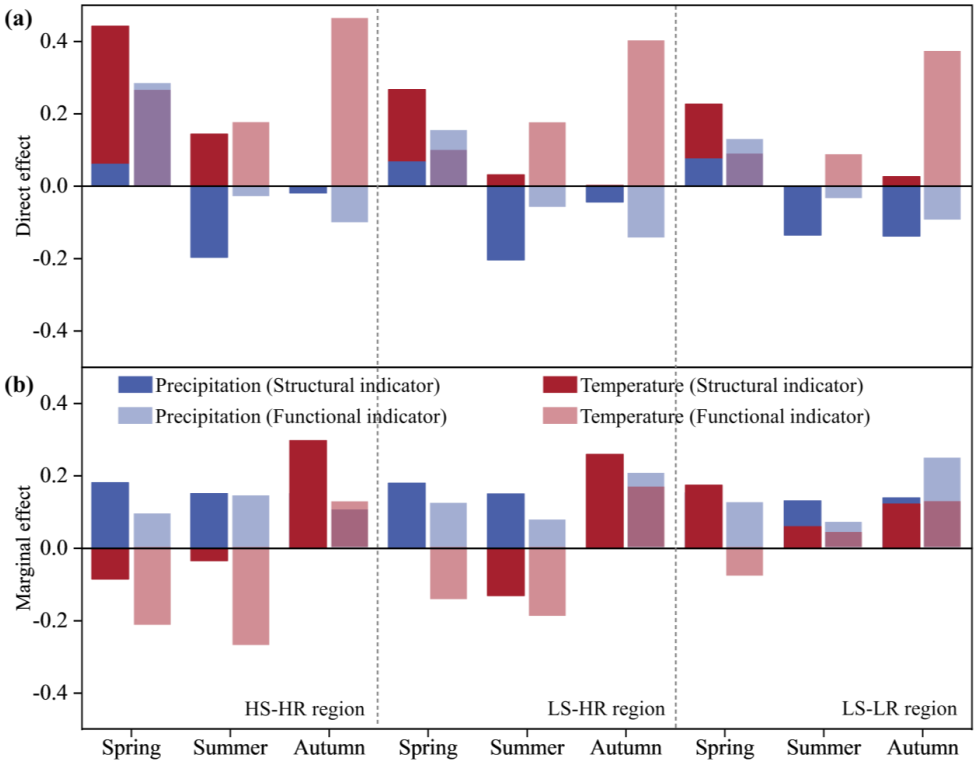

Figure 7 Seasonal direct and marginal effects of precipitation and temperature on vegetation metrics across hydro-lithological regions. (a) Direct effects of precipitation and temperature on structural and functional indicators across spring, summer and autumn in the HS–HR, LS–HR and LS–LR regions; (b) Marginal effects of precipitation and temperature on the CWD sensitivity of structural and functional indicators in each season and hydro-lithological region.

Table 1. Marginal effects of precipitation and temperature on the four vegetation indicators to CWD in each growth season and hydro-lithological region.

Interaction effect between climatic factor and climatic water deficit	Regions	Season	Structural indicators			Functional indicators		
			NDVI	EVI	Ensemble mean	GPP	SIF	Ensemble mean
Precipitation	HS-HR	Spring	0.21	0.08	0.18	0.20	−0.08	0.09
		Summer	0.04	0.16	0.15	0.31	−0.06	0.14
		Autumn	0.17	0.04	0.15	−0.06	0.23	0.10
	LS-HR	Spring	0.19	0.09	0.18	0.24	−0.07	0.12
		Summer	0.04	0.15	0.15	0.16	−0.01	0.08
		Autumn	0.13	0.06	0.12	0.01	0.34	0.21
	LS-LR	Spring	0.07	0.16	0.15	0.26	−0.08	0.13
		Summer	0.11	0.10	0.13	0.15	0.00	0.07
		Autumn	0.16	0.07	0.14	0.05	0.35	0.25
Temperature	HS-HR	Spring	−0.31	−0.26	−0.32	−0.25	0.20	−0.09
		Summer	0.01	−0.08	−0.07	−0.27	0.22	−0.03
		Autumn	−0.23	0.17	−0.04	0.06	0.33	0.30
	LS-HR	Spring	−0.19	−0.11	−0.16	−0.18	0.27	−0.01
		Summer	0.03	−0.04	−0.01	−0.27	0.12	−0.13
		Autumn	−0.27	0.11	−0.09	0.16	0.21	0.26
	LS-LR	Spring	−0.03	−0.01	−0.01	−0.06	0.41	0.17
		Summer	0.13	0.01	0.07	−0.14	0.26	0.06
		Autumn	−0.15	0.04	-0.07	0.12	0.03	0.12

https://doi.org/10.5194/egusphere-2026-2712
Preprint. Discussion started: 11 June 2026

3.3 Available bedrock water storage and a seasonal trade-off: buffering in summer, amplifying in transitional seasons

Available bedrock water storage ($S_{bedrock,cum}$) exhibited strong spatial variation across the Qinling Mountains (Figure 8). From 2000 to 2023, central and northern Qinling mountains steadily showed low $S_{bedrock,cum}$ (50–150 mm), while areas in the west and east had higher values (200–800 mm), which indicates greater reliance on bedrock water (Figure 8a). These spatial patterns in bedrock water storage corresponded to variations in hydro-lithological properties (Figure 8a). In particular, the mean $S_{bedrock,cum}$ varied from a peak of 379.1 mm in the LS-HR region to a low of 310.7 mm in the LS-LR region, with the HS-HR region characterised by a mean value of 348.6 mm. Such spatial divergence implies that the LS-HR region, which exhibits the highest $S_{bedrock,cum}$, functions as a key hydrological reservoir that supports greater canopy development than in the LS-LR region; it also yields vegetation development (such as NDVI, EVI and GPP) comparable to that in the water-rich HS-HR region (Figure 9).

Comparing the observed CWD sensitivity (β_1) with a counterfactual scenario excluding bedrock water showed distinct seasonal effects of bedrock water. In summer, structural sensitivity decreased from 0.026 to 0.022 in the HS-HR region and from 0.016 to 0.012 in the LS-HR region (Figure 8b), which suggests that bedrock-water access buffers increased canopy water demand during peak growth and thus attenuates sensitivity to CWD. This buffering is particularly amplified in the LS-HR region due to its limited soil water storage compared with the HS-HR region, which indicates that bedrock water serves as an indispensable resource for vegetation when surface water availability is restricted. By contrast, in the LS-LR region, where soil and regolith have limited water storage capacity, bedrock-water access decreased structural

https://doi.org/10.5194/egusphere-2026-2712
Preprint. Discussion started: 11 June 2026

sensitivity (−0.038 to −0.046). Although persistent water limitation likely constrains biomass accumulation in this region, even modest additional bedrock water can enhance greenness, which amplifies drought responses. This bedrock water-driven enhancement of greenness suggests a 'structural overshoot' mechanism, where vegetation develops canopy capacity beyond the sustainable water supply (Callahan et al., 2022; Chai et al., 2025; Li et al., 2023; Zhang et al., 2024). In addition, bedrock-water access made functional sensitivity more negative in the HS-HR and LS-LR regions (by 1.9% and 17.2%, respectively), but it dampened the positive functional sensitivity in the LS-HR region (by 3.4%). Therefore, in the HS-HR region, canopy development supported by bedrock-water access remains energy-limited in terms of structural greenness, whereas canopy functional activity has already shifted to water limitation ahead of structural greenness. Accordingly, in water-rich settings, even modest bedrock-water access can shift the dominant constraint on peak-season canopy development from energy limitation to water limitation. By contrast, in spring, bedrock-water access increased structural and functional sensitivities across all hydroclimatic regions (by 0.7% to 24.2%), underlining that bedrock water acts as an additional source that promotes early-season vegetation growth (McCormick et al., 2021; Stocker et al., 2023). However, it also heightened the responses of structural greenness and functional activity to water deficit. By the late growing season, vegetation dynamics were dominated by phenological progression, and the effect of bedrock-water access on functional and structural sensitivities was minimal (< 0.5%).

Overall, these results highlight lithology-driven bedrock water storage, along with the hydrological properties of soil–regolith, as the key mediators of vegetation–climate coupling. While bedrock water can buffer forests against drought in summer, it may also increase drought

https://doi.org/10.5194/egusphere-2026-2712
Preprint. Discussion started: 11 June 2026

sensitivity in spring and autumn by driving canopy 'structural overshoot'. This phenomenon demonstrates a seasonal trade-off between buffering and amplification across hydro-lithological settings, which explains the contrasting seasonal resilience and vulnerability of the monsoon Qinling mountains to CWD.

The hydro-lithological controls on seasonal drought responses were by no means confined to the Qinling Mountains. During the 2011–2017 drought in California's Sierra Nevada, spatially varied forest impacts and pronounced patchiness in stand structure and vulnerability were linked to variations in bedrock properties (Callahan et al., 2022). Accumulating evidence shows that woody plants can rely on bedrock water to sustain transpiration and carbon storage, which highlights regolith as a component of ecosystem water supply (Hahm et al., 2019, 2020, 2024; Liu et al., 2025; McCormick et al., 2021). Consistent with the mechanism identified here, bedrock composition and regolith properties also regulate ecosystem productivity sensitivity to hydroclimatic variability at global scales (Dong et al., 2023). This growing evidence highlights the necessity to incorporate subsurface hydrological heterogeneity, beyond the soil profile, in models predicting forest function under increasing hydroclimatic variability. From a management perspective, strategies should be tailored to specific hydro-lithological regions. For instance, in the HS-HR region with abundant water resources, promoting structural diversity may enhance carbon storage capacity while avoiding structural overshoot. In the LS-HR region, limiting vegetation cover could reduce the risk of widespread mortality during sudden drought events. In the LS-LR region, management should focus on drought-tolerant species and stand compositions due to the limited water supply. Incorporating hydro-lithological regionalisation and the dynamic role of bedrock water into management planning

https://doi.org/10.5194/egusphere-2026-2712
Preprint. Discussion started: 11 June 2026

may therefore mitigate drought impacts associated with unsustainable water use.

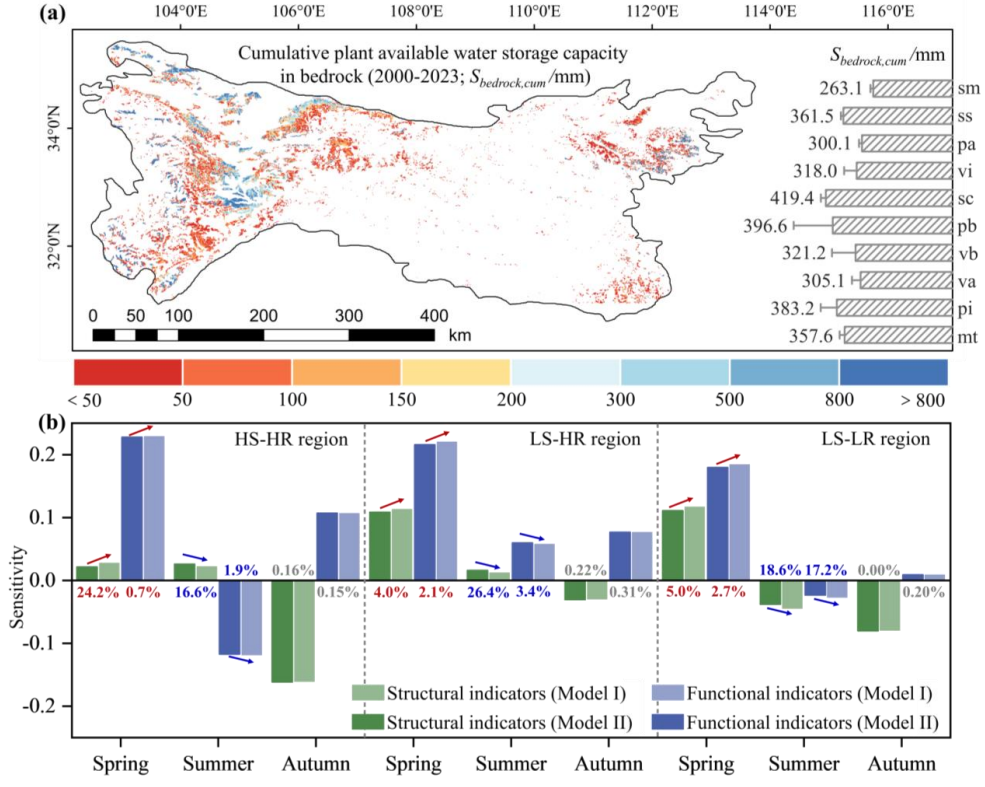

Figure 8 Spatial patterns of plant-available bedrock water storage and its influence on vegetation sensitivity to CWD. (a) Spatial distribution of cumulative plant-available bedrock water storage capacity in the Qinling Mountains (2000–2023; $S_{bedrock,cum}$). The bar chart shows mean $S_{bedrock,cum}$ for each lithological class; (b) Seasonal sensitivities of structural and functional indicators to CWD in the HS-HR, LS-HR and LS-LR regions. Sensitivities are estimated using two models: Model I, which includes bedrock-water access (Equation 1), and Model II, which excludes bedrock-water storage (Equation 4). Bars show structural and functional sensitivities in spring, summer and autumn for each model. Arrows and percentages denote the relative change in sensitivity in Model I compared with Model II, which is calculated as $2(\beta_1$-

https://doi.org/10.5194/egusphere-2026-2712
Preprint. Discussion started: 11 June 2026

461 $\beta_{1s}/(\beta_1+\beta_{1s})$, where β represents the estimated sensitivity coefficients.

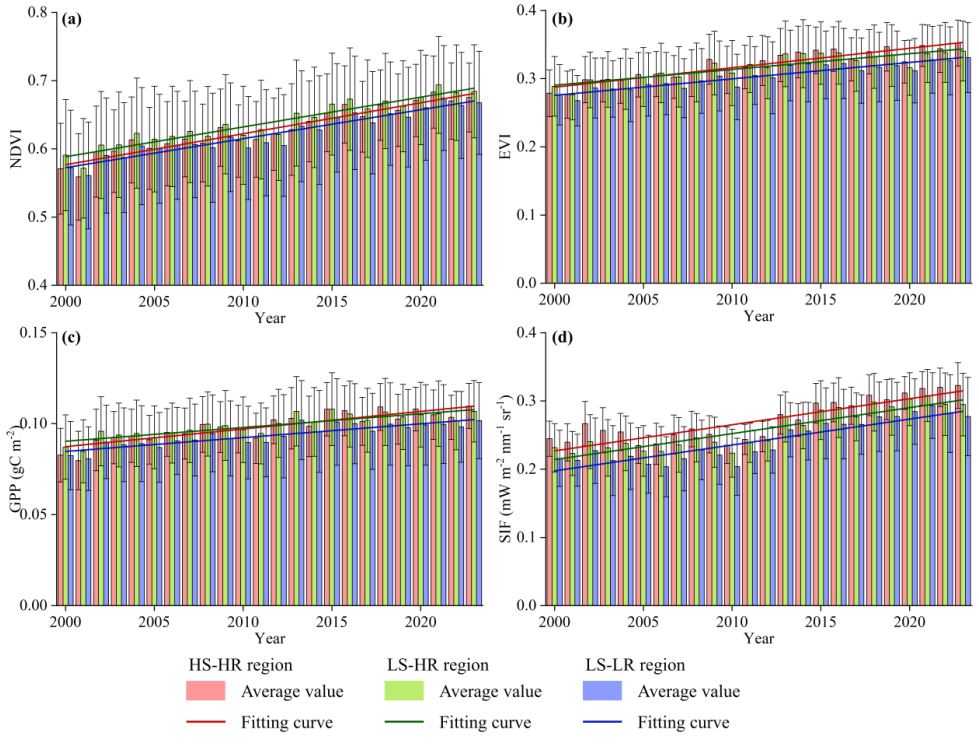

462

463 Figure 9 Temporal variations of vegetation indicators across the three hydro-lithological regions

464 (HS-HR, LS-HR and LS-LR). (a) NDVI; (b) EVI; (c) GPP; (d) SIF.

465 **3.4 Uncertainty and limitations**

466 Several uncertainties and limitations should be considered when interpreting the results of

467 this study. Firstly, the bedrock-water contribution estimated here is not a direct observation of

468 water stored in fractured bedrock, but an inferred subsidy derived from a water-balance

469 framework. In this framework, when monthly evapotranspiration demand exceeds the

470 combined supply from contemporaneous precipitation and antecedent soil water storage, the

471 resulting shortfall is attributed to plant-accessible deep subsurface water. Importantly, previous

472 studies have shown that bedrock-stored water can also be utilized even when precipitation and

https://doi.org/10.5194/egusphere-2026-2712
Preprint. Discussion started: 11 June 2026

soil moisture are sufficient, particularly in regions characterized by shallow soils or deep-rooted plant species (Ding et al., 2021; Qiu et al., 2026). Accordingly, the inferred bedrock-water subsidy should be interpreted as a conservative estimate.

Secondly, the hydro-lithological regionalisation is based on a threshold classification of soil available water capacity and a rank-based regolith storage–transmission index derived from porosity and permeability. This classification is intended to capture the major contrasts in water storage and transmission potential across the Qinling Mountains, rather than to fully resolve the continuous heterogeneity of subsurface hydraulic properties within each lithological class. This framework is primarily designed to reveal spatial and seasonal contrasts in the role of inferred bedrock-water subsidy in modulating vegetation sensitivity to climatic water deficit (CWD).

Finally, the results are best interpreted as regional-scale ecohydrological patterns consistent with lithologically mediated subsurface water regulation, rather than as direct evidence of bedrock-water use at individual grid cells. Nevertheless, the spatial and seasonal patterns observed across hydro-lithological regions strongly indicate that subsurface water storage and accessibility play a critical role in modulating forest sensitivity to climatic water deficit—effects that extend well beyond the Qinling Mountains. Future work integrating flux observations, isotopic tracing, bedrock-moisture monitoring, and process-based modelling will help to better constrain the underlying mechanisms.

4. Conclusion

This study demonstrates that lithology exerts a strong seasonal control on forest sensitivity to climatic water deficit in the Qinling Mountains by regulating the storage, accessibility, and ecological consequences of bedrock water. Forest functional activity was more responsive to

https://doi.org/10.5194/egusphere-2026-2712
Preprint. Discussion started: 11 June 2026

CWD than canopy greenness, revealing a pervasive functional–structural decoupling and indicating that greenness-based assessments alone may underestimate hydrological stress. The climatic effect on the vegetation sensitivity to CWD was strongly season dependent: precipitation generally enhanced CWD sensitivity in summer and autumn, whereas warming reduced sensitivity in spring and summer, especially where soils and bedrock can store more water, but increased it in autumn. Most importantly, bedrock-stored water showed a dual effect. It buffered drought stress during peak summer growth by supplementing shallow water deficits, but it also increased sensitivity in spring by promoting canopy development and water demand. Thus, bedrock water does not simply increase resilience; it can also intensify later vulnerability through seasonal demand amplification. Overall, our results suggest that drought response in mountain forests is governed by a seasonal trade-off between hydrological buffering and ecological amplification, and that this trade-off is fundamentally conditioned by hydro-lithological properties of the soil–regolith system. These findings highlight the need to move beyond soil-only perspectives of plant-available water and to explicitly incorporate bedrock water and lithological heterogeneity into hydrological models, drought assessments, and forest management in mountain water-tower regions

Data Availability Statement

Monthly precipitation (https://www.tpdc.ac.cn/zh-hans/data/faae7605-a0f2-4d18-b28f-5cee413766a2), temperature (https://www.tpdc.ac.cn/zh-hans/data/71ab4677-b66c-4fd1-a004-b2a541c4d5bf/), potential evapotranspiration (https://www.tpdc.ac.cn/zh-hans/data/8b11da09-1a40-4014-bd3d-2b86e6dccad4/) and normalized difference vegetation index (https://www.tpdc.ac.cn/zh-hans/data/10535b0b-8502-4465-bc53-78bcf24387b3) for 2000-

https://doi.org/10.5194/egusphere-2026-2712
Preprint. Discussion started: 11 June 2026

2023 were obtained from the National Tibetan Plateau Data Centre. Monthly ET, GPP and EVI were obtained from the National Aeronautics and Space Administration (NASA) EarthData portal (https://search.earthdata.nasa.gov/search). The LHSIF dataset was from Zenodo (https://doi.org/10.5281/zenodo.16394372; Zou et al., 2025). The 1:1,000,000 Vegetation Map of China was obtained from the Resource and Environmental Science Data Center (https://www.resdc.cn/data.aspx?DATAID=122). Available water content data were obtained from the global HiHydroSoil v2.0 database (https://www.dropbox.com/scl/fo/nf2jgaz4mvdp0c8zcedla/AGzoL2LXMtktzJ93Y7ETjP8?rlkey=yhpw01sq62wp62zb59qh7mknn&e=1&dl=0). Soil thickness data were obtained from the National Earth System Science Data Center (http://soil.geodata.cn/ztsj.html), as described by Liu et al. (2022) and Liu et al. (2020). Lithological classes were obtained from the high-resolution Global Lithological Map database (GLiM; https://www.geo.uni-hamburg.de/en/geologie/forschung/aquatische-geochemie/glim.html). Regolith porosity and permeability were obtained from the Global HYdrogeology MaPS (GLHYMPS; https://emf.creaf.cat/external_data/glhymps/).

Acknowledgement

The authors gratefully acknowledge the financial support from the National Natural Science Foundation of China (Grant Nos. 42341101 and 42522705).

Author contribution

TQS: Conceptualization, Methodology, Data curation, Formal analysis, Investigation, Software, Validation, Visualization, Writing – original draft; QYM: Conceptualization, Methodology, Supervision, Project administration, Funding acquisition, Resources, Writing – review &

https://doi.org/10.5194/egusphere-2026-2712
Preprint. Discussion started: 11 June 2026

539 editing; JLL: Methodology, Formal analysis, Validation, Writing – review & editing; YZ: Data
540 curation, Resources, Investigation, Writing – review & editing; XYS: Data curation, Software,
541 Validation, Visualization, Writing – review & editing; HQ: Resources, Investigation, Writing –
542 review & editing; DH: Supervision, Project administration, Resources, Writing – review &
543 editing; JBP: Conceptualization, Supervision, Funding acquisition, Project administration,
544 Writing – review & editing.

545 **Competing interests**

546 The contact author has declared that none of the authors has any competing interests.

547 **Reference**

548 Callahan, R. P., Riebe, C. S., Sklar, L. S., Pasquet, S., Ferrier, K. L., Hahm, W. J., et al.: Forest
549 vulnerability to drought controlled by bedrock composition, Nat. Geosci., 15, 714–719,
550 https://doi.org/10.1038/s41561-022-01012-2, 2022.

551 Chai, Y., Miao, C., AghaKouchak, A., Pokhrel, Y., Fu, Y., Li, X., et al.: Flash droughts
552 exacerbate global vegetation loss and delay recovery, Nat. Commun.,
553 https://doi.org/10.1038/s41467-025-67173-x, 2025.

554 Chen, Y., Zhou, Z., and Xu, C.: Transition from orogenic plateau to thinning reveals mesozoic
555 North China craton dynamics, Commun. Earth Environ., 6, 791,
556 https://doi.org/10.1038/s43247-025-02784-2, 2025.

557 Condon, L. E., Atchley, A. L., and Maxwell, R. M.: Evapotranspiration depletes groundwater
558 under warming over the contiguous United States, Nat. Commun., 11, 873,
559 https://doi.org/10.1038/s41467-020-14688-0, 2020.

560 Ding, Y., Nie, Y., Chen, H., Wang, K., and Querejeta, J. I.: Water uptake depth is coordinated

https://doi.org/10.5194/egusphere-2026-2712
Preprint. Discussion started: 11 June 2026

561 with leaf water potential, water-use efficiency and drought vulnerability in karst vegetation,
562 New Phytol., 229, 1339–1353, https://doi.org/10.1111/nph.16971, 2021.
563 Ding, Y. and Peng, S.: Spatiotemporal trends and attribution of drought across China from
564 1901–2100, Sustainability, 12, 477, https://doi.org/10.3390/su12020477, 2020.
565 Ding, Y. and Peng, S.: Spatiotemporal change and attribution of potential evapotranspiration
566 over China from 1901 to 2100, Theor. Appl. Climatol., 145, 79–94,
567 https://doi.org/10.1007/s00704-021-03625-w, 2021.
568 Dong, X., Martin, J. B., Cohen, M. J., and Tu, T.: Bedrock mediates responses of ecosystem
569 productivity to climate variability, Commun. Earth Environ., 4, 114,
570 https://doi.org/10.1038/s43247-023-00773-x, 2023.
571 Dossa, K., You, J., Wang, L., Zhang, Y., Li, D., Zhou, R., et al.: Transcriptomic profiling of
572 sesame during waterlogging and recovery, Sci. Data, 6, 204, https://doi.org/10.1038/s41597-
573 019-0226-z, 2019.
574 Ehlert, R. S., Hahm, W. J., Dralle, D. N., Rempe, D. M., and Allen, D. M.: Bedrock controls on
575 water and energy partitioning, Water Resour. Res., 60, e2023WR036719,
576 https://doi.org/10.1029/2023WR036719, 2024.
577 Fan, Y., Miguez-Macho, G., Jobbágy, E. G., Jackson, R. B., and Otero-Casal, C.: Hydrologic
578 regulation of plant rooting depth, Proc. Natl. Acad. Sci. USA, 114, 10572–10577,
579 https://doi.org/10.1073/pnas.1712381114, 2017.
580 Fu, Z., Ciais, P., Wigneron, J.-P., Gentine, P., Feldman, A. F., Makowski, D., et al.: Global
581 critical soil moisture thresholds of plant water stress, Nat. Commun., 15, 4826,
582 https://doi.org/10.1038/s41467-024-49244-7, 2024.

https://doi.org/10.5194/egusphere-2026-2712
Preprint. Discussion started: 11 June 2026

583 Gao, J., Shi, Y., Chen, X., Zhang, W., Shen, W., Xiao, T., and Zhang, Y.: China regional 250 m
584 normalized difference vegetation index data set (2000–2024), National Tibetan Plateau / Third
585 Pole Environment Data Center [data set], 2023.
586 Gleeson, T., Moosdorf, N., Hartmann, J., and Van Beek, L. P. H.: A glimpse beneath earth's
587 surface: GLobal HYdrogeology MaPS (GLHYMPS) of permeability and porosity, Geophys.
588 Res. Lett., 41, 3891–3898, https://doi.org/10.1002/2014GL059856, 2014.
589 Hahm, W. J., Dralle, D. N., Rempe, D. M., Bryk, A. B., Thompson, S. E., Dawson, T. E., and
590 Dietrich, W. E.: Low subsurface water storage capacity relative to annual rainfall decouples
591 Mediterranean plant productivity and water use from rainfall variability, Geophys. Res. Lett.,
592 46, 6544–6553, https://doi.org/10.1029/2019GL083294, 2019.
593 Hahm, W. J., Rempe, D. M., Dralle, D. N., Dawson, T. E., and Dietrich, W. E.: Oak transpiration
594 drawn from the weathered bedrock vadose zone in the summer dry season, Water Resour. Res.,
595 56, e2020WR027419, https://doi.org/10.1029/2020WR027419, 2020.
596 Hahm, W. J., Dralle, D. N., Lapides, D. A., Ehlert, R. S., and Rempe, D. M.: Geologic controls
597 on apparent root-zone storage capacity, Water Resour. Res., 60, e2023WR035362,
598 https://doi.org/10.1029/2023WR035362, 2024.
599 Hahm, W. J., Riebe, C. S., Lukens, C. E., and Araki, S.: Bedrock composition regulates
600 mountain ecosystems and landscape evolution, Proc. Natl. Acad. Sci. USA, 111, 3338–3343,
601 https://doi.org/10.1073/pnas.1315667111, 2014.
602 Hahm, W. J., Rempe, D. M., Dralle, D. N., Dawson, T. E., Lovill, S. M., Bryk, A. B., et al.:
603 Lithologically controlled subsurface critical zone thickness and water storage capacity
604 determine regional plant community composition, Water Resour. Res., 55, 3028–3055,

https://doi.org/10.5194/egusphere-2026-2712
Preprint. Discussion started: 11 June 2026

https://doi.org/10.1029/2018WR023760, 2019.

Hartmann, J. and Moosdorf, N.: The new global lithological map database GLiM: A representation of rock properties at the Earth surface, Geochem. Geophys. Geosyst., 13, 2012GC004370, https://doi.org/10.1029/2012GC004370, 2012.

Jiang, N., Shen, M., and Yang, Z.: Differential phenological responses to temperature among various stages of spring vegetation green-up, J. Plant Ecol., 17, rtae063, https://doi.org/10.1093/jpe/rtae063, 2024.

Jiao, W., Wang, L., Smith, W. K., Chang, Q., Wang, H., and D'Odorico, P.: Observed increasing water constraint on vegetation growth over the last three decades, Nat. Commun., 12, 3777, https://doi.org/10.1038/s41467-021-24016-9, 2021.

Jin, H., Vicente-Serrano, S. M., Tian, F., Cai, Z., Conradt, T., Boincean, B., et al.: Higher vegetation sensitivity to meteorological drought in autumn than spring across European biomes, Commun. Earth Environ., 4, 299, https://doi.org/10.1038/s43247-023-00960-w, 2023.

Keenan, T. F., Gray, J., Friedl, M. A., Toomey, M., Bohrer, G., Hollinger, D. Y., et al.: Net carbon uptake has increased through warming-induced changes in temperate forest phenology, Nat. Clim. Change, 4, 598–604, https://doi.org/10.1038/nclimate2253, 2014.

Leite, P. A. M., Rempe, D. M., McInnes, K. J., Schmidt, L. M., Walker, J. W., Olariu, H. G., and Wilcox, B. P.: Trees enhance rock moisture storage: A major pool in karst drylands and crucial during droughts, Water Resour. Res., 61, e2024WR038692, https://doi.org/10.1029/2024WR038692, 2025.

Li, W., Pacheco-Labrador, J., Migliavacca, M., Miralles, D., Hoek Van Dijke, A., Reichstein, M., et al.: Widespread and complex drought effects on vegetation physiology inferred from

https://doi.org/10.5194/egusphere-2026-2712
Preprint. Discussion started: 11 June 2026

627 space, Nat. Commun., 14, 4640, https://doi.org/10.1038/s41467-023-40226-9, 2023.
628 Li, X., Silvestro, R., Liang, E., Mencuccini, M., Camarero, J. J., Rathgeber, C. B. K., et al.:
629 Warming increases the phenological mismatch between carbon sources and sinks in conifers,
630 Nat. Clim. Change, 15, 1363–1370, https://doi.org/10.1038/s41558-025-02474-z, 2025.
631 Li, X., Piao, S., Huntingford, C., Peñuelas, J., Yang, H., Xu, H., et al.: Global variations in
632 critical drought thresholds that impact vegetation, Natl. Sci. Rev., 10, nwad049,
633 https://doi.org/10.1093/nsr/nwad049, 2023.
634 Lian, X., Piao, S., Li, L. Z. X., Li, Y., Huntingford, C., Ciais, P., et al.: Summer soil drying
635 exacerbated by earlier spring greening of northern vegetation, Sci. Adv., 6, eaax0255,
636 https://doi.org/10.1126/sciadv.aax0255, 2020.
637 Lian, X., Morfopoulos, C., and Gentine, P.: Water deficit and storm disturbances co-regulate
638 Amazon rainforest seasonality, Sci. Adv., 10, eadk5861, https://doi.org/10.1126/sciadv.adk5861,
639 2024.
640 Liu, F., Wu, H. Y., Zhao, Y. G., Li, D. C., Yang, J. L., Song, X. D., Shi, Z., Zhu, A. X., and
641 Zhang, G. L.: Mapping high-resolution National Soil Information Grids of China, Sci. Bull., 67,
642 328–340, https://doi.org/10.1016/j.scib.2021.10.013, 2022.
643 Liu, F., Zhang, G. L., Song, X. D., Li, D. C., Zhao, Y. G., Yang, J. L., Wu, H. Y., and Yang, F.:
644 High-resolution and three-dimensional mapping of soil texture of China, Geoderma, 361,
645 114061, https://doi.org/10.1016/j.geoderma.2019.114061, 2020.
646 Liu, M., Trugman, A. T., Peñuelas, J., and Anderegg, W. R. L.: Climate-driven disturbances
647 amplify forest drought sensitivity, Nat. Clim. Change, 14, 746–752,
648 https://doi.org/10.1038/s41558-024-02022-1, 2024.

https://doi.org/10.5194/egusphere-2026-2712
Preprint. Discussion started: 11 June 2026

649 Liu, T., Hu, Z., Zhang, D., Li, S., Cheng, C., Zhou, L., et al.: The timing of the initial collision
650 between the South and North China blocks constraining from the sediments in the eastern
651 Sichuan Basin, Sci. Rep., 13, 22378, https://doi.org/10.1038/s41598-023-49498-z, 2023.
652 Liu, X., Chen, X., Zhang, Z., Liu, W., Gao, F., Cheng, Q., et al.: The role of rock fractures as a
653 water source for trees growing in karst, Water Resour. Res., 61, e2024WR039588,
654 https://doi.org/10.1029/2024WR039588, 2025.
655 Liu, Y., Lian, J., Nie, Y., Wang, K., and Chen, H.: The role of root-zone soil moisture in delaying
656 vegetation responses to drought: Comparative insights from karst and non-karst areas, J.
657 Hydrol., 663, 134216, https://doi.org/10.1016/j.jhydrol.2025.134216, 2025.
658 Luo, Z., Fan, J., Shao, M., Yang, Q., and Li, M.: Rock moisture reinforces belowground water
659 storage under different precipitation scenarios and vegetation coverage, J. Hydrol., 636, 131276,
660 https://doi.org/10.1016/j.jhydrol.2024.131276, 2024.
661 McCormick, E. L., Dralle, D. N., Hahm, W. J., Tune, A. K., Schmidt, L. M., Chadwick, K. D.,
662 and Rempe, D. M.: Widespread woody plant use of water stored in bedrock, Nature, 597, 225–
663 229, https://doi.org/10.1038/s41586-021-03761-3, 2021.
664 McDowell, N. G., Allen, C. D., Anderson-Teixeira, K., Aukema, B. H., Bond-Lamberty, B.,
665 Chini, L., et al.: Pervasive shifts in forest dynamics in a changing world, Science, 368, eaaz9463,
666 https://doi.org/10.1126/science.aaz9463, 2020.
667 Miguez-Macho, G. and Fan, Y.: Spatiotemporal origin of soil water taken up by vegetation,
668 Nature, 598, 624–628, https://doi.org/10.1038/s41586-021-03958-6, 2021.
669 Mokhtar, A., He, H., Alsafadi, K., Li, Y., Zhao, H., Keo, S., et al.: Evapotranspiration as a
670 response to climate variability and ecosystem changes in southwest China, Environ. Earth Sci.,

https://doi.org/10.5194/egusphere-2026-2712
Preprint. Discussion started: 11 June 2026

79, 312, https://doi.org/10.1007/s12665-020-09007-1, 2020.

Nadal-Sala, D., Grote, R., Birami, B., Knüver, T., Rehschuh, R., Schwarz, S., and Ruehr, N. K.: Leaf shedding and non-stomatal limitations of photosynthesis mitigate hydraulic conductance losses in Scots pine saplings during severe drought stress, Front. Plant Sci., 12, 715127, https://doi.org/10.3389/fpls.2021.715127, 2021.

Ott, R. F.: How lithology impacts global topography, vegetation, and animal biodiversity: A global-scale analysis of mountainous regions, Geophys. Res. Lett., 47, e2020GL088649, https://doi.org/10.1029/2020GL088649, 2020.

Peng, S., Ding, Y., Wen, Z., Chen, Y., Cao, Y., and Ren, J.: Spatiotemporal change and trend analysis of potential evapotranspiration over the Loess Plateau of China during 2011–2100, Agric. Forest Meteorol., 233, 183–194, https://doi.org/10.1016/j.agrformet.2016.11.129, 2017.

Peng, S., Gang, C., Cao, Y., and Chen, Y.: Assessment of climate change trends over the Loess Plateau in China from 1901 to 2100, Int. J. Climatol., 38, 2250–2264, 2018.

Peng, S., Ding, Y., Liu, W., and Li, Z.: 1 km monthly temperature and precipitation dataset for China from 1901 to 2017, Earth Syst. Sci. Data, 11, 1931–1946, https://doi.org/10.5194/essd-11-1931-2019, 2019.

Piao, S., Wang, X., Park, T., Chen, C., Lian, X., He, Y., et al.: Characteristics, drivers and feedbacks of global greening, Nat. Rev. Earth Environ., 1, 14–27, https://doi.org/10.1038/s43017-019-0001-x, 2019.

Qiu, Y., Zhang, F., Gao, L., He, Z., Xiong, H., Peng, L., Wang, Z., Cui, H., Su, C., Zhang, D., Zhou, S., Ma, C., and Zhou, A.: Uncovering the dynamic role of bedrock-stored water in ecosystem evapotranspiration, J. Hydrol., 668, 134987,

https://doi.org/10.5194/egusphere-2026-2712
Preprint. Discussion started: 11 June 2026

https://doi.org/10.1016/j.jhydrol.2026.134987, 2026.

Rempe, D. M. and Dietrich, W. E.: Direct observations of rock moisture, a hidden component of the hydrologic cycle, Proc. Natl. Acad. Sci. USA, 115, 2664–2669, https://doi.org/10.1073/pnas.1800141115, 2018.

Running, S., Mu, Q., and Zhao, M.: MODIS/Terra net evapotranspiration 8-day L4 global 500 m SIN grid V061, NASA EOSDIS Land Processes Distributed Active Archive Center (DAAC), MOD16A2-061, 2021.

Simons, G. W. H., Koster, R., and Droogers, P.: HiHydroSoil v2.0 – A high resolution soil map of global hydraulic properties, FutureWater Report 213, FutureWater, Wageningen, the Netherlands, 2020.

Schmidt, L. and Rempe, D.: Quantifying dynamic water storage in unsaturated bedrock with borehole nuclear magnetic resonance, Geophys. Res. Lett., 47, e2020GL089600, https://doi.org/10.1029/2020GL089600, 2020.

Sreeparvathy, V., Debdut, S., and Mishra, A.: A review of advances in flash drought research: Challenges and future directions, Earth's Future, 13, e2025EF006603, https://doi.org/10.1029/2025EF006603, 2025.

Stocker, B. D., Tumber-Dávila, S. J., Konings, A. G., Anderson, M. C., Hain, C., and Jackson, R. B.: Global patterns of water storage in the rooting zones of vegetation, Nat. Geosci., https://doi.org/10.1038/s41561-023-01125-2, 2023.

Sun, W., Zhou, S., Yu, B., Zhang, Y., Keenan, T., and Fu, B.: Soil moisture-atmosphere interactions drive terrestrial carbon-water trade-offs, Commun. Earth Environ., 6, 169, https://doi.org/10.1038/s43247-025-02145-z, 2025.

https://doi.org/10.5194/egusphere-2026-2712
Preprint. Discussion started: 11 June 2026

715 Tian, S., Van Dijk, A. I. J. M., Tregoning, P., and Renzullo, L. J.: Forecasting dryland vegetation
716 condition months in advance through satellite data assimilation, Nat. Commun., 10, 469,
717 https://doi.org/10.1038/s41467-019-08403-x, 2019.
718 Vicca, S., Balzarolo, M., Filella, I., Granier, A., Herbst, M., Knohl, A., et al.: Remotely sensed
719 detection of effects of extreme droughts on gross primary production, Sci. Rep., 6, 28269,
720 https://doi.org/10.1038/srep28269, 2016.
721 Wang, Z., Fu, B., Wu, X., Li, Y., Feng, Y., Wang, S., et al.: Vegetation resilience does not
722 increase consistently with greening in China's Loess Plateau, Commun. Earth Environ., 4, 336,
723 https://doi.org/10.1038/s43247-023-01000-3, 2023.
724 Wu, J., Yang, Y., Yin, G., Zhao, J., Ding, T., and Zhao, W.: Greening nonlinearly intensifies
725 drought impacts on grasslands of the Qinghai–Tibet Plateau, Glob. Change Biol., 31, e70532,
726 https://doi.org/10.1111/gcb.70532, 2025.
727 Wu, M., Manzoni, S., Vico, G., Bastos, A., De Vries, F. T., and Messori, G.: Drought legacy in
728 sub-seasonal vegetation state and sensitivity to climate over the Northern Hemisphere, Geophys.
729 Res. Lett., 49, e2022GL098700, https://doi.org/10.1029/2022GL098700, 2022.
730 Xu, H., Chen, H. W., Chen, D., Wang, Y., Yue, X., He, B., et al.: Global patterns and drivers of
731 post-fire vegetation productivity recovery, Nat. Geosci., 17, 874–881,
732 https://doi.org/10.1038/s41561-024-01520-3, 2024.
733 Yang, Y.-M., Shin, J., Park, S.-W., Park, J.-H., An, S.-I., Kug, J.-S., et al.: Fast reduction of
734 Atlantic SST threatens Europe-wide gross primary productivity under positive and negative
735 CO2 emissions, npj Clim. Atmos. Sci., 7, 117, https://doi.org/10.1038/s41612-024-00674-6,
736 2024.

https://doi.org/10.5194/egusphere-2026-2712
Preprint. Discussion started: 11 June 2026

737 Zeng, Y., Hao, D., Park, T., Zhu, P., Huete, A., Myneni, R., et al.: Structural complexity biases
738 vegetation greenness measures, Nat. Ecol. Evol., 7, 1790–1798,
739 https://doi.org/10.1038/s41559-023-02187-6, 2023.
740 Zhang, W., Smith, W. K., Keenan, T. F., Dannenberg, M. P., Li, Y., Wang, S., et al.: Seasonal
741 stabilization effects slowed the greening of the Northern Hemisphere over the last two decades,
742 Nat. Commun., 16, 6287, https://doi.org/10.1038/s41467-025-61308-w, 2025.
743 Zhang, X., Wang, X., Zohner, C. M., Peñuelas, J., Li, Y., Wu, X., et al.: Declining precipitation
744 frequency may drive earlier leaf senescence by intensifying drought stress and enhancing
745 drought acclimation, Nat. Commun., 16, 910, https://doi.org/10.1038/s41467-025-56159-4,
746 2025.
747 Zhang, Y., Liu, L., Cheng, Y., Kang, S., Li, H., Wang, L., et al.: Intensified structural overshoot
748 aggravates drought impacts on dryland ecosystems, Earth's Future, 12, e2023EF003977,
749 https://doi.org/10.1029/2023EF003977, 2024.
750 Zhao, J., Paschalis, A., Gentine, P., Feng, Z., and Fatichi, S.: Limited capability of current
751 satellite solar-induced chlorophyll fluorescence reconstructions to capture stomatal responses
752 to environmental stresses, Commun. Earth Environ., 7, 9, https://doi.org/10.1038/s43247-025-
753 03035-0, 2025.
754 Zou, C., Du, S., Liu, X., and Liu, L.: Development of the Long-term Harmonized multi-satellite
755 SIF (LHSIF) dataset at 0.05° resolution (1995–2023), Earth Syst. Sci. Data Discuss.
756 https://doi.org/10.5194/essd-2025-94, 2025.